

### **3-D Numerical Study of Impinging Water Jets in Run Out Table Cooling Processes**

Dr. Myung Jong Cho  
POSCO Technical Research Labs.  
1 Goedong, Nam-gu, Pohang city, Kyung-buk, South KOREA  
Phone – (054) 220-9237

Dr. Brian G. Thomas  
University of Illinois at urbana-champaign.  
1206 west Green St., Urbana, IL, 61801  
Phone – (217) 333-6919

Dr. Pil Jong Lee  
POSCO Technical Research Labs  
Phone – (054) 220-9237

Key words : Run Out Table, Cooling, Hot Rolling Process, CFD

#### **INTRODUCTION**

Controlled cooling<sup>[1,2]</sup> from the impingement of water jets is used in many commercial processes to optimize the microstructure and properties of metal products. In the ROT (Run Out Table) cooling process after hot rolling, steel producers have developed many new technologies<sup>[3-6]</sup> to lower production costs, to continuously improve product quality, and even to create new microstructures, in order to fulfill the increasing demands of customers. For example, to produce higher strength steel with less alloying elements, technology to increase the cooling rates is of growing interest.

Several technologies<sup>[6-9]</sup> to increase the cooling rate in the ROT have been recently developed. Ultra-fast cooling technology<sup>[6,7]</sup> increases the conventional cooling rate of 30 ~ 80°C/s, depending on the final thickness, to 300°C/s on 4mm thick hot strip. An acceleration cooling technology<sup>[8,9]</sup> having more than 200°C/s on 3mm thick makes it possible to increase the strength of steel or to achieve the same level of strength with a low carbon equivalent design. These technologies use larger flow rates than conventional cooling methods (such as spray or water column cooling), basically. In the ultra-fast cooling, total water flow is well known as 17,000 L/min per m<sup>[6]</sup> of cooling length. This corresponds to 9,200 L/min-m<sup>2</sup> assuming a 1.8m width<sup>[7]</sup>, which is more than double the maximum flow rate for the conventional ROT cooling<sup>[6]</sup>.

The tools to develop these technologies include models of transient heat conduction in the moving strip<sup>[10]</sup>. They rely on heat transfer coefficients between the impinging water jets and the strip surface, which are generally obtained from plant measurements<sup>[10, 11]</sup>. The design of better cooling header systems requires knowledge of these heat transfer coefficients as a function of the flow conditions, which depend on header configuration, nozzle geometry, spacing, height, flow rate, and other parameters. This knowledge is generally obtained from lab-scale experiments that must be further verified with full-scale prototypes in expensive plant experiments. Thus, there is a strong need for fundamentally-based tools to predict surface heat transfer in the real process.

There has been much previous work<sup>[12-16]</sup> on heat transfer from impinging jets (including free, confined, and submerged), based on experimental, analytical and numerical studies. However, water impingement from multiple jets onto moving surfaces, and for the high flow-rate conditions of real ROT cooling has received much less attention. Specifically, these conditions involve the development of free gas-liquid surfaces and flow in the liquid pool above a high-temperature metal surface, where complex boiling, steam-layer development, and Leidenfrost effects occur. Heat transfer depends greatly on the details of the flow conditions, in addition to the surface temperature. A first step in fundamental study of these complex phenomena is to quantify the location and depth of the free surface of the liquid pool. Recently, Gradeck et al.<sup>[17]</sup> studied the free-surface of the water pool formed from a

single water jet impinging on a moving surface. They investigated the water jump position both numerically and experimentally for conditions chosen to simulate a conventional ROT cooling process.

In this article, the flow pattern and free surface arising from multiple water jets impinging on a moving surface within the flow rate region of ROT process has been simulated numerically, and validated with measurements. Specifically, the effects of surface width and increasing flow rate have been investigated, and a general equation to predict the water pool depth has been developed.

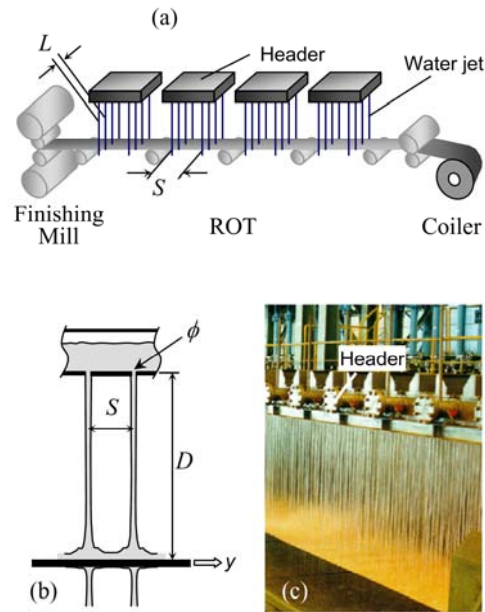


Figure 1. Cooling process on the run out table

## ROT COOLING PROCESS

**Figure 1** shows a typical ROT cooling process, and close-up schematic of two adjacent water jets. As the steel strip moves from the hot rolling mill to the coiler, it passes under banks of cooling nozzles called “headers”. Cooling water pours through each nozzle with diameter  $\phi$  and forms a continuous stream of water that impinges onto the moving steel strip. It spreads over the moving surface. Similar cooling jets impinge from below the strip, not shown in **Figure 1(c)** for clarity. Heat transfer is influenced by the accumulation of a water pool on the moving strip. This is investigated by simulating the fluid flow pattern, velocity and pressure distribution in this water pool and the shape of its free surface beneath a representative portion of the impinging water jets.

## NUMERICAL PROCEDURE

In this article, the standard conservation equations for steady-state incompressible mass and momentum conservation were calculated in a representative portion of the ROT, solving the standard Navier-Stokes equations in three-dimensions. Inlet boundary condition at the entrance from each nozzle is fixed normal velocity  $V_j$ . The volume of fluid model (VOF) was adopted to calculate the shape of the free surface of the water pool due to the water jets impinging on the moving surface. An advanced interface capturing technique known as High Resolution Interface Capturing (HRIC) was selected for tracking the free surface with reduced numerical diffusion. This interface capture scheme can be used to the steady state problem as well as transient ones. It was well known<sup>[18]</sup> that this scheme gives more efficient convergence to the final steady state solution than other robust schemes based on transient solvers such as Donor-Acceptor<sup>[19]</sup> or Geometric Reconstruction Scheme<sup>[20]</sup>. A boundary condition of  $VOF_w = 1$  was assumed at each inlet plane, indicating that the nozzle exit was filled with cooling water.

The standard  $k-\epsilon$  model was used for turbulence closure and the wall function approach was adopted at the surface of the moving strip, where normal velocity is zero and the tangential boundary condition is the strip velocity. Pressure boundary conditions of 0 MPa gage are imposed on the non-nozzle portions of the top surface where  $VOF_w = 0$  and on the free sides of the domain. The convection and diffusion terms of the governing equation were discretized using the 2<sup>nd</sup> order upwind scheme. The SIMPLE algorithm was employed to calculate the pressure. All computations were carried out using Fluent software (release 6.2.16).

## VERIFICATION THROUGH SINGLE-JET TEST CASES

To test the accuracy of the present computational model, the experiment of Gradeck et al.<sup>[17]</sup> for a single water jet impinging onto a moving surface was simulated. As shown in **Figure 2**, the water jet issues from a 17mm diameter inlet located 60mm above the moving surface, flows through a larger (22-mm) diameter development region, and impinges perpendicularly onto the moving surface. **Figure 3** shows the 150mm×250mm×60mm numerical grid of 117,000 cells and the boundary conditions employed. The first cells adjacent to the domain bottom were chosen in the region of  $y^+ = 10 \sim 40$  (the lower limit for accurate wall function performance) to obtain a fine grid system near the moving surface. A uniform grid spacing of 5mm in the z-direction was adopted to facilitate capture of a sharp free surface.

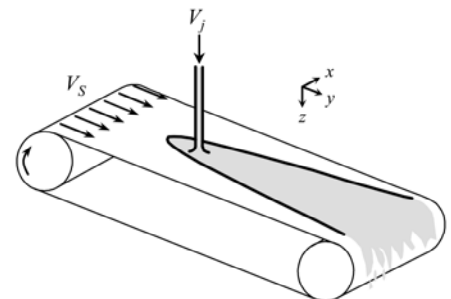


Figure 2. A schematic view of the single water jet experiment<sup>[15]</sup>

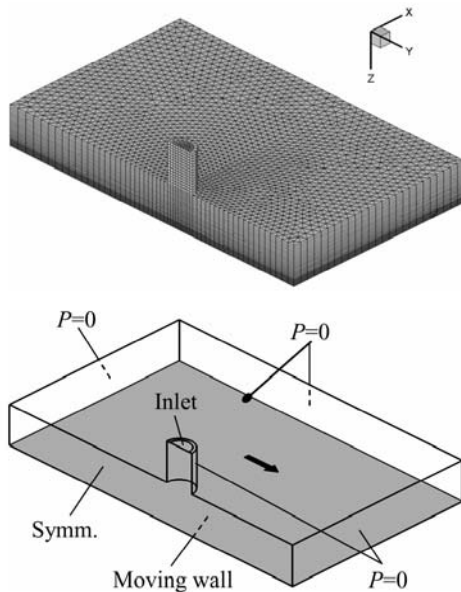


Figure 3. Domain and boundary conditions for single-water jet verification problem

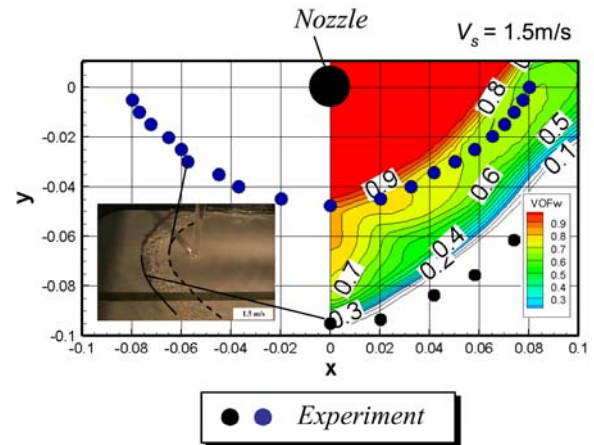


Figure 4. Simulated volume fraction contours compared with measurement of hydraulic jump position and photo<sup>[15]</sup> (single water jet experiment)

Results of the calculated volume fraction of water ( $VOF_w$ ) on the moving surface are compared in **Figure 4** with the experimental hydraulic jump position for the case of strip velocity  $V_s=1.5\text{m/s}$  and jet velocity  $V_j=1\text{m/s}$ . In this figure, it was found that the edges of the hydraulic jump region were in good agreement with the contours of  $VOF_w=0.8$  and  $0.2$ , respectively. In this comparison, it was thought that the range of  $VOF_w=0.2 \sim 0.8$  could approximately represent the bubble region in this highly turbulent, mixed flow

problem. It was assumed that  $VOF_w=0.2$  was the proper value to define the free surface. In **Figure 5**, photographs of the free surfaces of three cases with different surface moving speeds ( $V_s=0.5, 1.0$  and  $1.5\text{m/s}$ ) were compared the calculated iso-surfaces of  $VOF_w=0.2$ . Increasing speed naturally causes the hydraulic jump region to move closer to the jet, and to curve more. As shown in this figure, the calculated  $VOF_w$  iso-surfaces agree reasonably well with the experimental free surface shapes. The predicted maximum water pool depths (in the hydraulic jump region) were 3.34, 3.64, and 5.32mm for these 3 velocities, which appears again to match reasonably well with the measured results in **Figure 5**.

These findings show that the present computational model can quantitatively predict the shape of the free surface in an accumulated water pool on a moving surface, including the bubbles induced by the turbulent flow from an impinging water jet, with reasonable accuracy.

## RESULTS

The validated model was then applied to simulate the flow, pressure, and free-surface shape of the accumulated pool in a real ROT, after steady-state conditions have been established. To approximate the flow pattern and profile that develops after in long banks of nozzles, a representative repeating portion of the process was chosen for the computational domain.

It includes a double-row of nozzles and part of the overflow region at the edge of the strip.

This computational domain is a bank of nozzles near the middle of the ROT which is far enough from the first and the last nozzle banks that end effects can be ignored. **Figure 6** shows the domain and boundary conditions, which takes advantage of symmetry about the center-plane. Because this domain typically repeats in the moving direction (y-direction in **Figure 6**) to cover the entire cooling region of the real ROT process in **Figure 1** (about 20-200 times), the flow velocities entering the upstream plane of the

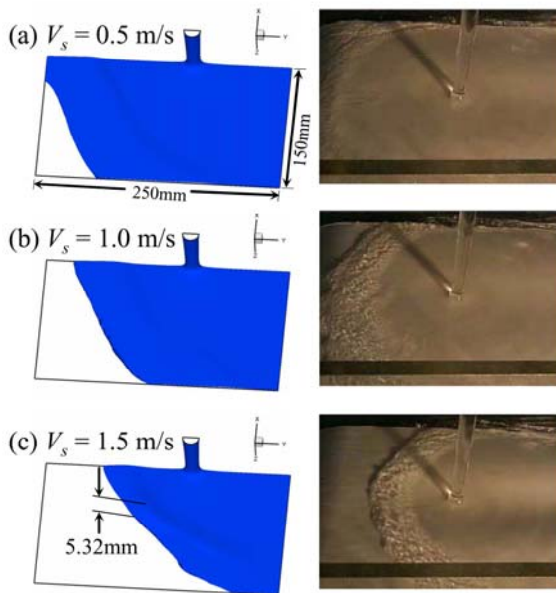


Figure 5. Comparison of the free surface shape for the different surface velocities (3D view) used for model verification

domain should roughly match those exiting the downstream plane. Therefore, the boundary condition for the two  $z$ - $x$  planes was adopted to be periodic. The nozzles were arranged in a typical zigzag pattern with the same pitch, ( $S=L$ ), as shown in **Figure 6**. The velocity at the nozzle exit was determined according to the desired flow rate, the number of nozzles in the area, and their outlet diameter. The domain includes the entire height of the nozzle outlet above the moving strip, which allows the model to capture the acceleration of each falling jet and the corresponding decrease in jet area, which matches the Bernoulli equation. To ensure that the outlet boundary conditions do not affect the inner flow pattern, the domain was extended to include beyond where the water and air drain from the side. The grids were concentrated near the moving surface on the basis that the first cell near the wall has  $y^+ = 10 \sim 40$ . A total of 824,000 cells were arranged for the 300mm width case.

#### (A) Conditions

Water flow rates per unit area range from 2,400 L/min- $m^2$  (60% of the capacity of a conventional ROT cooling process), to a maximum flow rate of 9,200 L/min- $m^2$  for the high-flow rate ROT process.<sup>[6,7]</sup> Computations were carried out specifically for 2400, 4800, 7200 and 9200 L/min- $m^2$ . The nozzle diameter ( $\phi$ ), spacing ( $S$ ) and pitch ( $L$ ) were fixed at 8.3mm, 30mm and 30mm for all of the calculations, respectively. The speed of moving surface (strip) was fixed at 10m/s (600mpm) and the height ( $D$ ) of the nozzle above the moving surface was assumed to be 500mm.

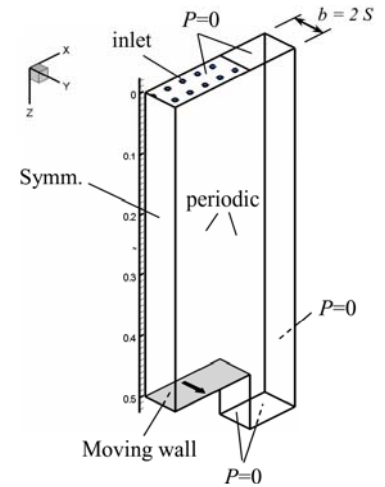


Figure 6. Calculation domain and the associated boundary conditions (3D view) used for model verification

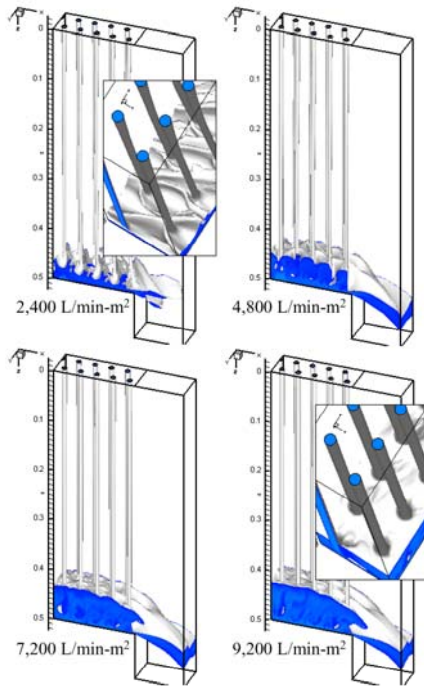


Figure 7. Effect of flow rate on the calculated free surface shape ( $W=300$ mm)

#### (B) Flow Rate Effect

**Figure 7** shows the calculated iso-surfaces of  $VOF_w=0.2$  for 300mm width. In the case of 2,400 L/min- $m^2$ , each impinging jet makes its own hydraulic jump. When the flow rate increases above 2,400 L/min- $m^2$ , the hydraulic jump diminishes, making the surface smoother. In addition, the water pool height increases. Increasing flow rate from 2,400 L/min- $m^2$  to 9,200 L/min- $m^2$ , the maximum height of the free surface ( $VOF_w=0.2$ ) increases from 20mm to 77mm.

#### (C) Flow Pattern

**Figure 8** shows the typical flow pattern in the pool caused by the water jets, through tracers and velocity vectors for the 300mm, 9,200 L/min- $m^2$  case. The water columns all bend according to the bottom surface motion, causing flow recirculation and turbulence in the bottom of the pool. The bulk flow of water draining also bends the water columns, with increasing effect towards the edge of the strip. The air above the free surface ( $VOF_w=0.2$ ) is clearly shown to have high velocities and recirculation as well.

#### (D) Pressure

**Figure 9** and **10** present the calculated pressure contours and maximum pressure on the moving surface. Each jet creates a pressure peak that is stronger towards the strip edge, where the pool depth is less. From the classic Bernoulli equation, the maximum impact pressure of a free water jet should be proportional to the square of the nozzle exit velocity or the flow rate. However, **Figure 10** shows that this effect saturates, and the maximum pressure does not increase much for flow rates over

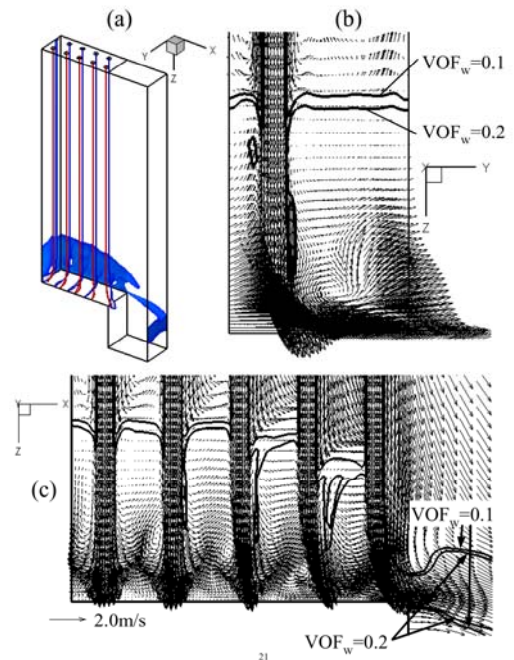


Figure 8. Calculated results ( $w=300$ mm, 9,200 L/min- $m^2$ )

- (a) vector tracers & region of  $VOF_w > 0.2$
- (b) velocity vectors and  $VOF_w$  contours at  $x=30$ mm
- (c) velocity vectors and  $VOF_w$  contours at  $y=15$ mm



7,000 L/min-m<sup>2</sup>. This is because the deeper water pool absorbs the impact energy of the water jet.

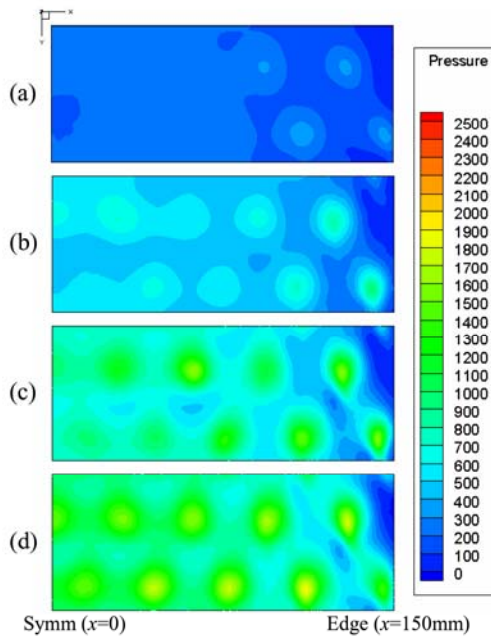


Figure 9. Calculated pressure contours on the moving surface (W=300mm)  
 (a) 2,400 L/min-m<sup>2</sup> (b) 4,800 L/min-m<sup>2</sup>  
 (c) 7,200 L/min-m<sup>2</sup> (d) 9,200 L/min-m<sup>2</sup>

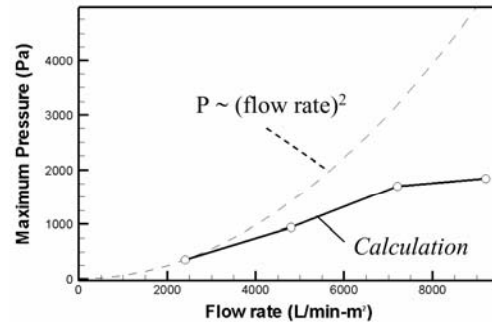


Figure 10: Calculated maximum pressure on the moving surface (W=300mm)

#### (E) Width Effect

Next, simulations were performed for different surface widths (300, 600, 900 and 1200mm) at constant flow rate (9,200 L/min-m<sup>2</sup>). The predicted free surface of the standard 300mm case is compared with the 1200mm case in **Figure 11**. Although the overall shape of the water pool is nearly the same, increasing width causes a deeper water pool height. Specifically, the pool height increases from 77 to 224mm. This is because the total water flow increases in proportion to the width, for the same water flow rate per unit area. This flow must traverse a longer distance past more nozzles in a wide

strip before it can reach and escape from the free edge.

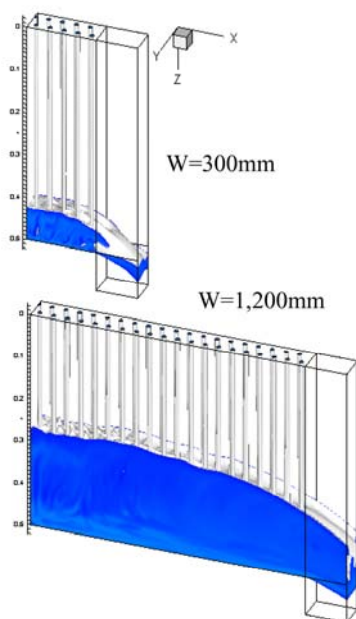


Figure 11. Free surface shapes calculated for two different strip widths. (9,200 L/min-m<sup>2</sup>)

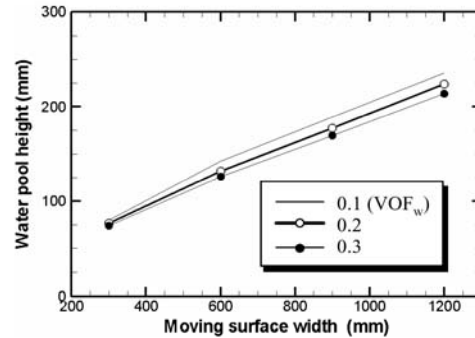


Figure 12. Effect of strip width and volume fraction of water on pool height (9,200 L/min-m<sup>2</sup>)

The calculated maximum height of the volume fractions from each simulation is plotted in **Figure 12**. The effect of the free surface criterion ( $VOF_w=0.2$ ) is shown to be small, as the free surface height does not vary much for the range of  $VOF_w = 0.1 \sim 0.3$ . Volume fraction contours that are close together is generally indicative of a more reliable numerical solution.

The calculated pressure distributions for each width case are compared in **Figure 13**. The pressure can be divided into two components: the minimum or “hydraulic” pressure ( $P_h$ ), and a pressure peak ( $\Delta P$ ), as shown in **Figure 13**. For 300m width, a strong pressure peak is found beneath each impinging jet. As width increases, this pressure peak drops and disappears. However, the hydraulic

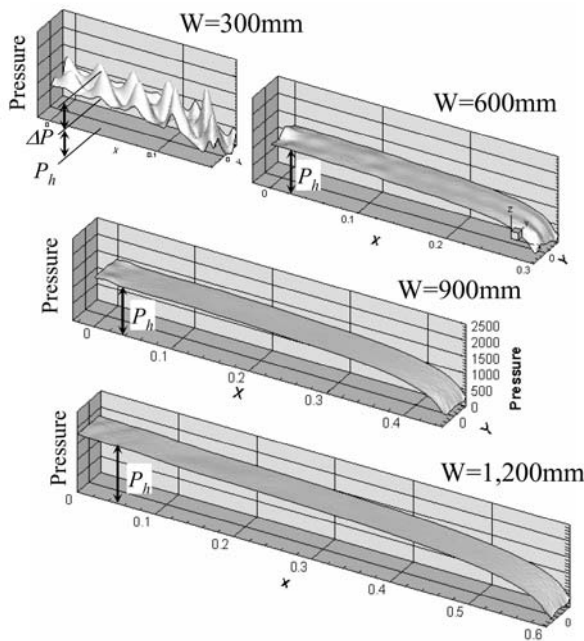


Figure 13. Calculated pressure distributions on the moving surface (9,200 L/min-m<sup>2</sup>)

following relation<sup>[21]</sup> between the total flow rate and water pool height for the open channel system was adopted to the present flow problem.

$$H(m) = C_d^{-2/3} \cdot b(m)^{-2/3} \cdot g^{-1/3} \cdot Q(m^3/s)^{2/3} \quad (1)$$

where

$Q$  : total flow rate (m<sup>3</sup>/s), as shown in **Figure 15**

$C_d$  : drag coefficient according to the weir shape

$b$  : weir length or water drain width (m), as shown in **Figure 15**

$g$  : 9.81 m/s<sup>2</sup>

$H$  : water pool height (m).

Tuning the unknown coefficient  $C_d$  with the calculated result for the 1200mm case,  $C_d$  was calculated to be 0.275. Lenz<sup>[22]</sup> developed  $C_d$  formula for the flow in **Figure 15(b)** as a function of  $H$  and  $Y$ . Specifically, decreasing weir height  $Y$  causes decreasing  $C_d$ . As an example,  $C_d$  drops from 0.544 to 0.275 as  $Y$  decreases from  $3.7 \cdot H$  to  $0.25 \cdot H$ . Because the present drain behavior is similar to **Figure 15(b)** with a small  $Y$ , the calculated  $C_d=0.275$  is thought to be reasonable.

The equation (1) was then re-arranged into a practical prediction tool. First,  $Q$  and  $b$  are expressed in terms of plant process parameters:

$$Q(m^3/s) = q(L/min)/1000/60 \cdot W(m)/2 \cdot 2 S(m) / L(m) / S(m) \quad (2)$$

$$b(m) = 2 S(m). \quad (3)$$

Flow rate per unit area,  $F$ , is defined as:

$$F(L/min-m^2) = q(L/min) / L(m) / S(m) \quad (4)$$

where

$q$  : flow rate per one nozzle (L/min)

$W$  : width of moving surface (m)

$L$  : spacing between nozzles in width direction (m)

$S$  : spacing between nozzles in moving (length) direction (m).

Inserting Eqs. (2)-(4) into equation (1), rearranging in terms of  $H$  and combining  $C_d$  and  $g$ , gives:

pressure increases proportionately with the water pool depth, roughly according to In **Figure 14**, the hydraulic pressure and the maximum difference in pressures  $\Delta P$  across the center region ( $x=0 \sim 150$ mm) are plotted for these four different width cases according to the water pool height. From this figure, it is clear that increasing the height of the water pool, causes more of the impinging force of the water jet to be absorbed. Although the hydraulic pressure and the average pressure both increase, this effect causes the pressure difference to decrease.

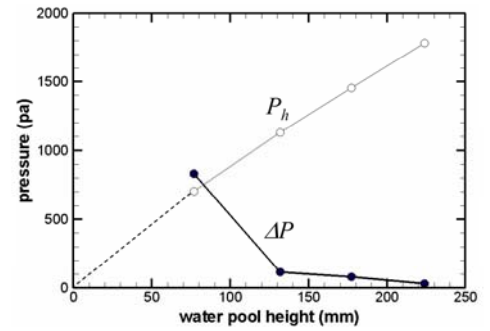


Figure 14. Calculated pressure peak and hydraulic pressure on the moving surface (9,200 L/min-m<sup>2</sup>)

### SIMPLE RELATION to Predict Pool Height

The two open-channel flows over weirs sketched in **Figure 15** have a similar draining mechanism with the present flow problem. Therefore, the

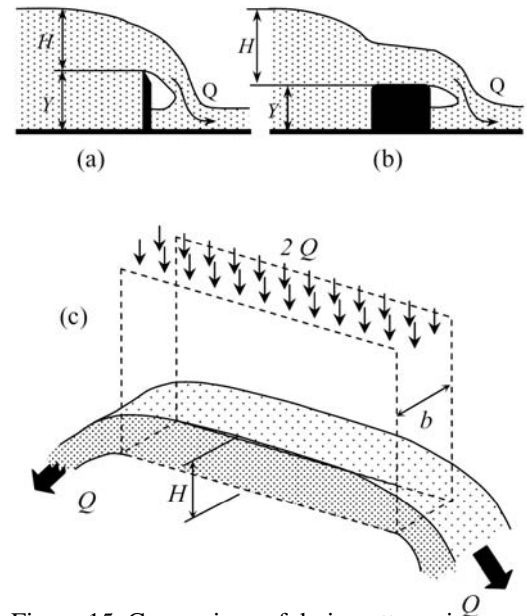


Figure 15. Comparison of drain patterns in (a) open channel flow over a thin weir (b) channel flow over thick weir (c) run out table

$$H(\text{mm}) = 0.454 \cdot [F(\text{L/min-m}^2) \cdot W(\text{m})]^{2/3}. \quad (5)$$

The predictions of equation (5) are compared with those of the 3-D model in **Figure 16**. In this figure, very good agreement is found.

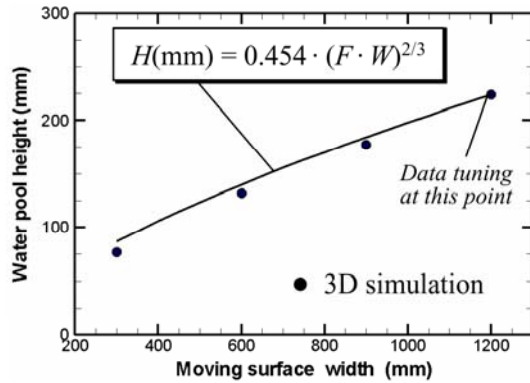


Figure 16: Comparison of water pool height calculation (9,200 L/min-m<sup>2</sup>)

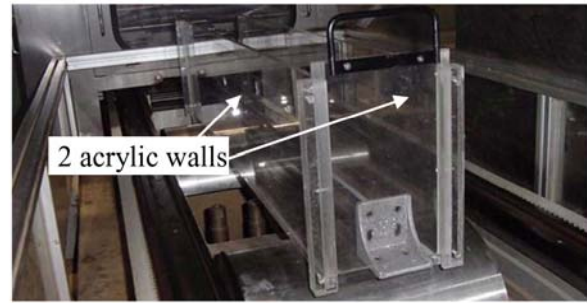


Figure 17: Water pool height experiment

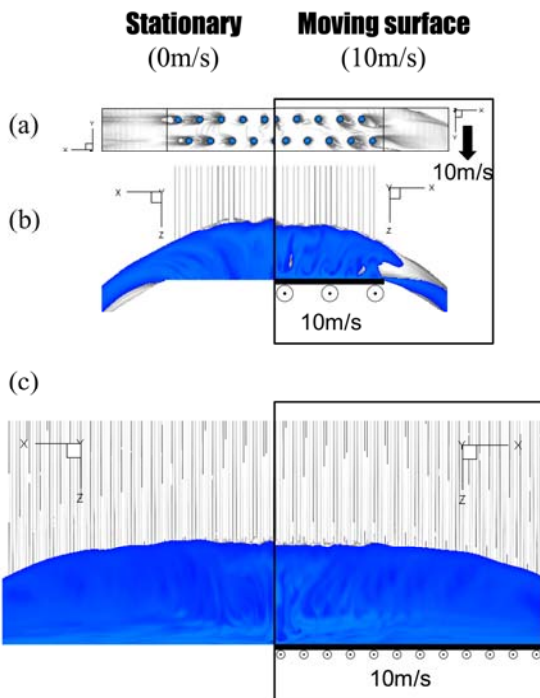


Figure 18: water pool height comparison between stationary and moving surface  
 (a) W=300mm (top view)  
 (b) W=300mm (front view)  
 (c) W=1,200mm

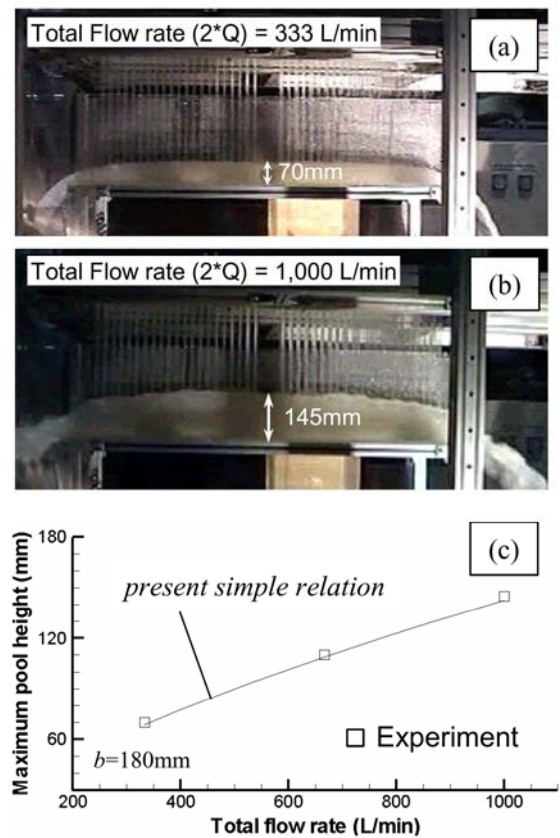


Figure 19: Comparison of water pool height

## EXPERIMENTAL VALIDATION OF SIMPLE RELATION

To verify the above relation between flow rate and pool height, a water model experiment, shown in **Figure 17**, was considered. This model has a stationary bottom, while the current work was based on the bottom surface moving at 10m/s. Thus, the effect of the bottom surface speed on the pool height was investigated first.

The free surfaces ( $VOF_w=0.2$ ) of a new stationary-bottom simulation (9,200 L/min-m<sup>2</sup>) and the corresponding moving case (10m/s)

are compared in **Figure 18**. The dips around the water columns of the moving surface case are elongated toward both the surface moving direction and the edge, whereas the dips in the stationary case elongate straight towards the edge, as shown in **Figure 18(a)**. The maximum water pool heights of stationary cases are just slightly greater than those of the moving cases (86mm vs 77mm for 300mm and 232mm vs 224mm for 1200mm). This difference of less than 9mm caused by the surface speed is not very significant relative to the natural variations in the surface profile caused by the turbulent flow.

Next, the predictions of the empirical equation were compared with measurements of the water pool height in the water model experiment, for two different flow rates. **Figure 19(a)** and **(b)** show photos of experiments for a total flow rate = 333 L/min (1,545 L/min-m<sup>2</sup>) and 1,000L/min (4,635 L/min-m<sup>2</sup>). These photos reconfirm that the water pool forms and contains bubbles. The water pool decreases in height towards the opening at the side. This is the same tendency as the model predictions (see **Figure 18**). In **Figure 19(c)**, the experiment water pool height was compared with that of the present relation. Variations in free surface height of 1-5mm are caused by each water jet, as seen in both the water experiments and in the computations. Within the uncertainty of these natural variations, the relation developed in this work between the pool height, flow rate and width agrees very well with the experiment.

## IMPLICATIONS FOR HEAT TRANSFER

The previous sections have presented a model for predicting the water pool depth that has been validated with experimental measurements. This provides an indication of the ability of the model to predict flow and pressure variations in the water pool, which is a crucial step in predicting heat transfer at the water / strip interface. This work is also useful in providing an initial indication of heat transfer in real processes. Generally, a deeper water pool would be expected to increase heat transfer, owing to the increased water available to remove heat. However, for very deep water pools, for the same flow conditions, heat transfer may decrease, owing to the increased uniformity of the pressure and flow fields, which makes steam removal more difficult. This has important practical implications: for example, increasing strip width at high water flow rates likely causes the heat transfer to decrease due to the water pool height increase. Without accounting for this, laboratory experiments may differ from the real plant.

Comparisons of heat transfer between top and bottom of the strip confirms that the relationship between pool depth and heat transfer is not simple, as many other phenomena are involved. Thus, much further work is needed: a comprehensive fundamental model of water vaporization, steam layer development, boiling heat transfer is being developed as future work.

## CONCLUSIONS

In this paper, impinging water jets on a moving surface has been numerically studied to investigate flow behavior in a realistic range of ROT processes. The 3-D  $k-\epsilon$  Reynolds Averaged Navier Stokes model features a second-order accurate discretization and the VOF method with High Resolution Interface Capturing scheme to handle the free surface flow and was implemented in Fluent 6.2.16. The model accurately predicted the free-surface shape in a verification problem of a single impinging water jet experiment using a volume fraction of 0.2 to define the free surface.

The velocities, free surface shape, and pressure on the moving surface were calculated for various flow rates and strip widths. The results show that increasing flow rate over 2,400 L/min-m<sup>2</sup>, causes a deep water pool to accumulate on the moving surface. The water pool depth increases with increasing strip width and increasing flow rate. It was also found that the pressure peak below each water jet decreases as the water pool height increases.

Based on the similarity in drainage flow behavior of the present problem with open-channel flow over a dam, a simple equation was derived to predict pool height from the water flow rate, nozzle spacings, and strip width. Pool height predictions using the simple equation agree well with those of water model experiments as well as the 3-D computations. The flow results have important implications for heat transfer in ROT processes, which are discussed briefly in preparation for further work.

## ACKNOWLEDGMENT

The authors would like to express their sincere gratitude to Prof. Gradeck for his help in providing the single water jet experimental data for the verification.



## REFERENCES

1. Z.D. Liu, I.V. Samarasekera : *J. of Iron and Steel Research International*, 2004, vol.11, pp.15-23.
2. J. Sengupta, B.G. Thomas and M.A. Wells : *Metall. Trans. A*, 2005, vol.36, pp.187-204.
3. Arvedi and Siemens VAI team : *Steel Times International*, 2006, vol.30, p 23.
4. J.A. Kromhout, A.A. Kamperman, M. Kick, F. Mensonides : *Ironmaking and Steelmaking*, 2006, vol.33, pp.362-366.
5. K. Sekiguchi, Y. Anbe, H. Imanari : *Trans. of the Institute of Electrical Engineers of Japan*, 2004, vol.124D, pp.190-195.
6. J.C. Herman : *Ironmaking and Steelmaking*, 2001, vol.28, pp.159-163.
7. A. Lucas, P. Simon, G. Bourdon, J.C. Herman, P. Riche, J. Neutjens and P. Harlet : *Steel Research International*, 2004, vol.75, pp.139-146.
8. F. Akio and O. Kazuo : *JFE Technical Report*, 2005, No.5, pp.10-15.
9. F. Akio, I. Sadanori, H. Yoshimich, M. Toru, M. Yoichi and I. Shozo : *EP patent application*, 2002, EP 1 210 993 A1.
10. C.G. Sun, H.N. Han, J.K. Lee, Y.S. Jin and S.M. Hwang : *ISIJ International*, 2002, vol.42, pp.392-400.
11. M.A. Smith and K. Weinzierl : *Iron & Steel Technology*, 2007, vol.4, pp.108-118.
12. B.W. Web, C.F. Ma : *Adv. Heat Transfer*, 1995, vol.26, pp.105-217.
13. J.H. Lienhard : *Ann. Rev. Heat Transfer*, 1995, pp.199-270.
14. S.V. Garimella : *Ann. Rev. Heat Transfer*, 2000, pp.413-494.
15. A.T. Hauksson, D. Fraser, V. Prodanovic, I.V. Samarasekera : *Ironmaking and Steelmaking*, 2004, vol.31, pp.51-56.
16. Z.D. Liu, D. Fraser, I.V. Samarasekera : *Canadian Metallurgical Quarterly*, 2002, vol. 41, pp.63-74.
17. M. Gradeck, A. Kouachi, A. Dani, D. Arnoult And J. L. Borean : *Experimental Thermal and Fluid Science*, 2006, vol.30, pp.193-201.
18. Fluent Inc. : *Tips & Tricks Fluent MAT Enews March*, 2005.
19. C.W. Hirt, B.D. Nichols : *J. of Computational Physics*, 1981, vol.39, pp.201-225.
20. D.L. Youngs : *Numerical Methods for Fluid Dynamics*, Academic, New York, NY, 1982.
21. F.M. White : *Fluid Mechanics*, 5th edition, McGraw Hill, New York, NY, 2003, pp.724-726.
22. A.T. Lenz : *ASCE Trans.*, 1943, vol.108, pp.759-802.